Case Temperature Monitoring-Based Online Condition Monitoring of SiC MOSFET Power Modules using a Radial Basis Function Network

Cameron Entzminger, Wei Qiao, and Liyan Qu
Power and Energy Systems Laboratory
Department of Electrical and Computer Engineering
University of Nebraska-Lincoln
Lincoln, NE 68588-0511 USA
centzminger@unomaha.edu; wqiao3unl.edu; lqu2@unl.edu

***Abstract*—Silicon carbide (SiC) metal-oxide-semiconductor field-effect transistor (MOSFET) power modules are being used for high power applications because of their superior thermal characteristics and high blocking voltage capabilities over traditional silicon power modules. This paper explores monitoring the temperature distribution of the baseplate of an SiC MOSFET power module for online condition monitoring of the power module. A radial basis neural network (RBFN) is trained to follow the operational temperature data of a healthy power module. As a module deteriorates the temperature distribution changes as well. Comparing the trained RBFN output and an unhealthy module's temperature output at the same point, the differences in temperature signify deterioration in the health of the module. The proposed method of online condition monitoring is applied to an SiC MOSFET power module and validated by computer simulations using finite element analysis models for the power module in both healthy and unhealthy conditions.**

Keywords—Condition monitoring, metal-oxide-semiconductor field-effect transistor (MOSFET), radial basis function network (RBFN), power module, silicon carbide (SiC), thermal modeling

I. Introduction

Power modules contain power semiconductors that are used for high power applications, such as three-phase inverters in medium-voltage drives or wind turbines. Silicon carbide (SiC) is a wide-bandgap semiconductor material being used for its efficient thermal conductivity characteristics and high blocking voltage capabilities [1]. All SiC metal-oxide-semiconductor field-effect transistor (MOSFET) power modules have recently been used as a replacement of their all silicon predecessors. Both types of power semiconductors are subject to some of the same factors of deterioration, such as electrical stress, power cycling, and mechanical vibration [2], [3]. The power semiconductors inside the power modules are mounted on a series of different layers of materials to provide efficient cooling, electrical isolation from the baseplate, and structural rigidity [4], [5]. The mismatch of thermal expansion coefficients between the different materials used in the semiconductor mounting layers causes each layer to expand by a different amount during a power cycling event. This mismatch of expansion causes mechanical stresses at the interfaces of each mismatched layer. Existing cracks in the solder layers grow with each thermal expansion event due to the mechanical stresses at the layer interfaces [6]. Larger cracks in the solder layer can manifest as a constriction of the heat conduction path from the semiconductor chips to the baseplate [7]. Constriction of the heat conduction path can cause overheating in the semiconductor chips. This overheating results in a buildup of mechanical stresses at the solder joints of the bond wires, leading to bond wire lift-off and failure of the power module [8], [9]. Constriction of the heat conduction path also results in changes in the temperature distribution across the baseplate of the power module.

During the operation of a power module, the switching and conduction losses in the semiconductor chips conduct through the power module with a certain heat flow path, causing a specific temperature distribution for a healthy module. Thermomechanical fatigue is the dominant failure mechanism experienced by the packaging materials in a power module [10]. A healthy module without any cracks in the solder layer conducts heat differently than an unhealthy module with cracks. A direct way of measuring for solder fatigue is to monitor the temperature directly in the solder layer or at different points inside the module. However, power modules are manufactured to optimize power density and lower cost and adding these sensors would increase the size and manufacturing cost of the module [11]. Therefore, a non-invasive means of measuring this change in heat flow is needed. Since cracks in the solder layers cause constriction of the heat flow path from the semiconductor chips to the baseplate, which causes a change in the temperature distribution across the baseplate of the power module, a method for identifying deviations in the temperature distribution across the baseplate of the power module can be used to monitor for solder cracks in the power module.

Solder fatigue in insulated-gate bipolar transistor (IGBT) power modules has been identified non-invasively by monitoring for changes in the temperature distribution across the baseplate in the IGBT power modules [12], [13]. However,

This work was supported in part by the U.S. National Science Foundation under Grant CMMI-1663562.

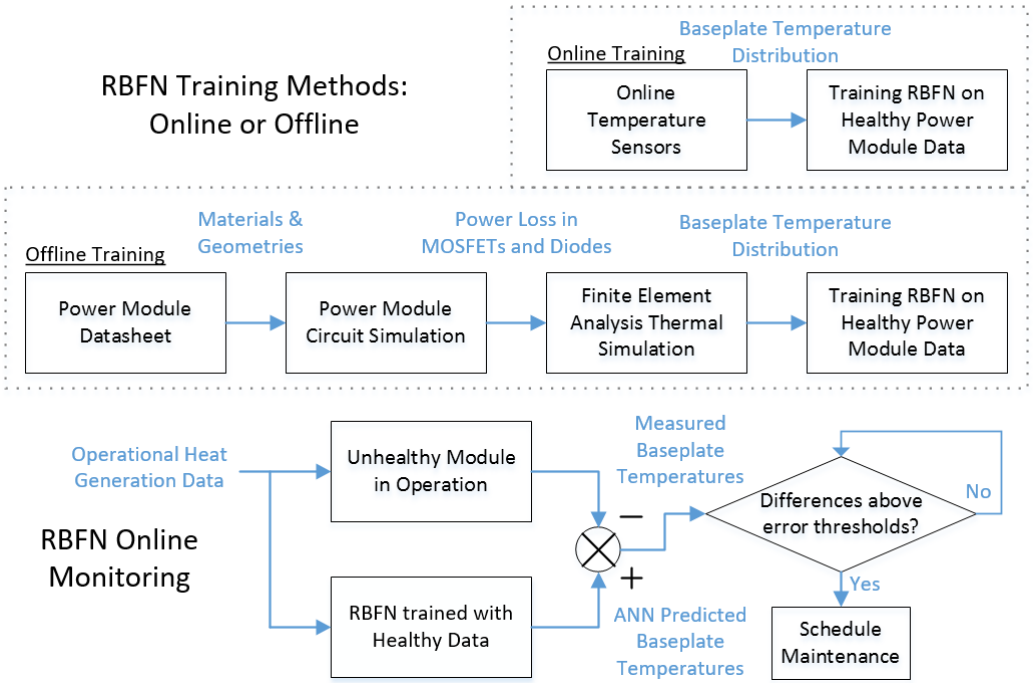

Fig. 1. Flowchart of the proposed method.

current case temperature monitoring methods do not scale the temperature sensing parameters automatically for different operating conditions. Current case temperature monitoring methods also do not account for the changes in temperature distribution at different points in time during a power module's operation which can aid the diagnosis of solder fatigue. Artificial neural networks (ANNs), such as radial basis function network (RBFN) can be used for function approximation applications [14]-[16]. One application of function approximation would be learning the change in temperature at a point on the baseplate of a healthy power module over the course of its normal operation. ANNs can learn complex relationships given an ample supply of training data. The relationship between the baseplate temperature and the heat generation at the semiconducting chips for multiple operational states of a power module can be taught to an ANN using training data gathered from a finite element analysis (FEA) simulation of a healthy power module. This allows for the consideration of the time-varying temperature across the baseplate for different operating states when diagnosing solder fatigue.

This paper proposes an RBFN-based online condition monitoring method for SiC MOSFET power modules. In the proposed method, an RBFN is trained to approximate and follow the case temperature at a specific point on a healthy power module's baseplate over the full operational range. The trained RBFN is then used online to estimate the case temperature at the same point on the power module during operation. If the health status of the power module deteriorates with significant solder cracks, a difference between the measured case temperature from the unhealthy power module and the output of the RBFN trained on the health power module is expected to be observed. This difference in case temperature can be used to identify deterioration in the power module device, thus resulting in a non-invasive means of online condition monitoring for a power module device.

The remainder of the paper is organized as follows. Section II presents the proposed method for online condition monitoring of power modules using an RBFN trained either online or offline. Section III presents the FEA simulation results and the RBFN training results for three different points on the baseplate of a simulated SiC MOSFET power module. Section IV discusses the final conclusions and future work related to these topics.

II. Proposed Method

An overview of the proposed method can be seen in Fig. 1. An RBFN can be trained either offline or online which differ in methodology and data used for training. For online training, an RBFN can use temperature data gathered directly from the device using temperature sensors while the device is in operation. For offline training, there is no device in operation for direct data sensing. Therefore, training data can instead be generated by simulating the device using computer aided design (CAD) software, performing power loss analysis using circuit simulation software, and then generating the resulting temperature data by performing a thermal analysis of the device regarding the power loss using FEA software. Training of an RBFN is performed the same way regardless of the data being used.

A trained RBFN is used for online monitoring to diagnose solder fatigue during real-time operation of a power module. This is performed by first obtaining the operational heat generation data of the power module by calculating the power

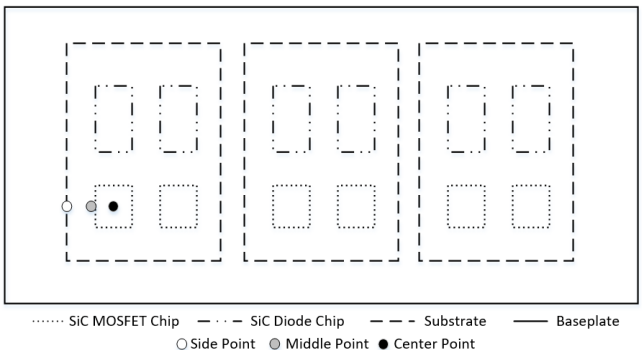

Fig. 2. Side, middle, and center baseplate temperature monitored points.

loss of the semiconductor chips during the power module's operation. An RBFN is trained to take the operational heat generation data as an input across the entire operational range of the power module and output the resulting temperature of a healthy power module at a specified monitoring point on the baseplate of the modules. Three monitoring points were used to diagnose the health of the module: the point on the baseplate directly below the center point of the semiconducting MOSFET chip, the point on the baseplate to the side of the center point of the chip directly below the edge of the solder layer, and the midpoint on the baseplate between these two points. The three points as seen in Fig. 2 were selected for judgement of the effects of solder cracking. If the module is healthy, then the monitoring temperature will match the RBFN output at each of the monitoring points. If there are unhealthy cracks in the solder layer, then for each point when compared to the RBFN output, the point beneath the center of the chip will have a greater temperature, the point at the edge of the solder layer will have a lower temperature, and the midpoint between these two points will not have a significant deviation in temperature. If these differences are each above a specified error tolerance, then the device should be scheduled for maintenance.

For offline training of the RBFN, a CAD model of a power module can be constructed using CAD software. The dimensions and materials of a power module can be obtained from a manufacturer datasheet and used to build a CAD model of the power module. The module's operating parameters, such as blocking voltage, conducting current, switching frequency, and average switching and conducting losses can be used in circuit simulation software to calculate the heat generation on a semiconductor chip during its operation. FEA software can then be used to perform a thermal analysis of the power loss resulting from the circuit simulation using the CAD model. The power loss calculated at each semiconducting chip of an SiC MOSFET power module is a heat generation input for the FEA simulation. The output of the FEA simulation is the temperature at each point in the mesh of the thermal model. For a healthy module, the solder layer has a specified length, width, and thickness in the module. In an unhealthy module, solder cracks grow from the outside of the layer inwards. After a significant period of wear, the cracks cause an increase in thermal impedance on the outer area of the solder layer, thus

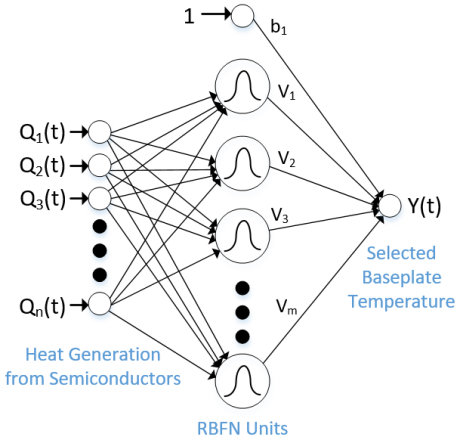

Fig. 3. RBFN expanded diagram.

constricting the heat flow towards the inside of the solder layer resulting in an increase in temperature below the chip on the baseplate and a decrease in temperature at the point below edge of the solder layer on the baseplate.

An RBFN is composed of three layers, the input layer, the hidden layer, and the output layer [17], [18]. The hidden layer consists of any number of units where each unit is fed an input vector and calculates a Gaussian density function which is a localized basis function. The outputs of all the units are then weighted and summed with corresponding bias values individually for the specified number of outputs. The Gaussian density function with a center vector C, input vector x, and scalar width parameter β can be seen in (1).

$$\varphi(x) = e^{\left(-\frac{\|x-C\|^2}{\beta^2}\right)} \tag{1}$$

For this application, each MOSFET and diode used in a power module has a corresponding heat generation curve associated with it. Each of these heat generation curves is an input to the RBFN as seen in Fig. 3 where Q_i ($i = 1, \cdots, n$) is the heat generation input of the ith semiconductor chip and n specifies the number of MOSEFTs and diodes. There is only one output, the temperature at the selected point on the baseplate, specified as Y in Fig. 3. After specifying how many units to use for an RBFN and accumulating a large amount of input data to train the RBFN, the algorithm k-means clustering can be used to find the optimal place for the centers of the units so that the centers can be positioned in a way that the distance from each input vector to a center is at a minimum for all input patterns. Once the center positions of the units are found, the widths of the units can be calculated using the P-nearest neighbors heuristic algorithm. This calculates the optimal width for each node by calculating the root-mean-squared distance or 2-norm, from a centroid to its neighbors using (2) where β is the width, i is the unit number, C is a center value, p is the number of neighbors being considered, and j is the index for the summation.

$$\beta_i = \left(\frac{1}{p}\sum_{j=1}^{p}\left\|C_i - C_j\right\|^2\right)^{1/2} \tag{2}$$

Once the centers and widths are calculated for a given number of units, the values are fixed and the weights $V = [b_1,$

$V_1, \cdots, V_m$] of the RBFN are calculated using the pseudoinverse method expressed by (3)-(7).

$$\hat{Y} = GV \tag{3}$$

$$g_{ij} = \varphi(x_i) = e^{\left(-\frac{\|x_i - c_j\|^2}{\beta_j^2}\right)} \tag{4}$$

$$Y \approx \hat{Y} \tag{5}$$

$$V = G^{-1}Y \tag{6}$$

$$V = (G^T G)^{-1} G^T Y \tag{7}$$

where the element of the matrix G in (3) is defined in (4) which is the result of each unit's Gaussian distribution function output in response to an input pattern; the weight matrix V in (3) determines $\hat{Y}$, the output of the RBFN; the vector C and scalar β in (4) are the center and width of the unit, respectively. The training procedure becomes an optimization problem of minimizing the difference between the healthy module output and the calculated RBFN output. In this case, the healthy module output is the simulated FEA solution of the chip temperature over a certain period. If the actual output was the same as the RBFN output, then Y would be equal to $\hat{Y}$. Thus, the optimal weights V would be obtained by (6) by multiplying the inverse of G by Y. Usually the inverse of G is not a square matrix, so the pseudoinverse can be used by first creating a square matrix using G then multiplying it by Y as shown in (7). Using the resulting weights in V from (7), this pseudoinverse method can be used to find the output of the RBFN.

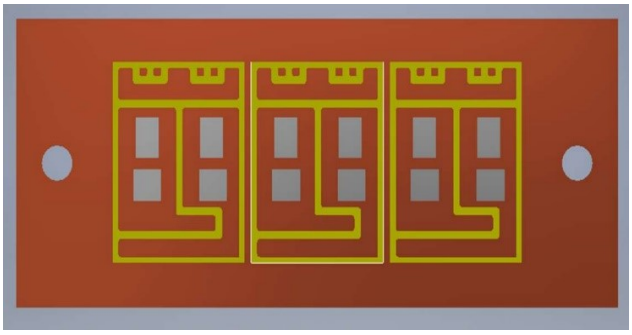

Fig. 4. Autodesk Inventor CAD model of a CREE CCS050M12CM2 SiC MOSFET power module.

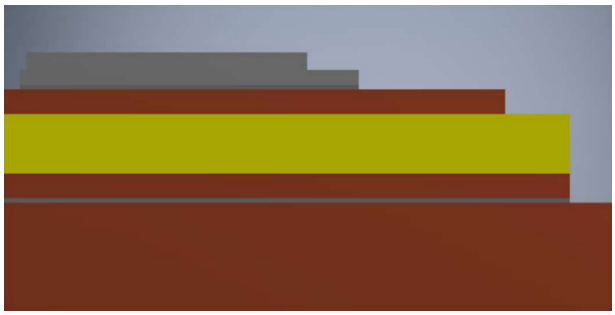

Fig. 5. Side view of a healthy power module.

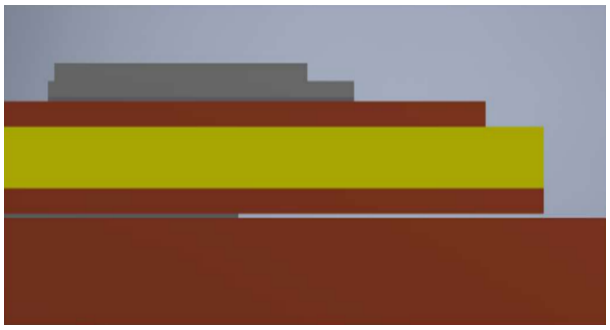

Fig. 6. Side view of an unhealthy power module.

III. Results and Discussion

Shown in Fig. 4 is the CAD model used for simulating an SiC MOSFET power module. The module was created in Autodesk Inventor which is a CAD design program freely available to students. The module's dimensions and material properties are based off the datasheet parameters listed for the CREE CCS050M12CM2 All-SiC Six-Pack Module [19]. There are three material stacks each for a single phase of a three-phase inverter. The power module geometry measurements and material properties are listed in [20]. Each material stack has its own solder to baseplate layer that was reduced in volume to simulate appropriate wear in the solder layer. Shown in Fig. 5 is the cross-sectional view of a healthy power module while shown in Fig. 6 is the cross-sectional view of an unhealthy power module. The solder layer in the unhealthy power module

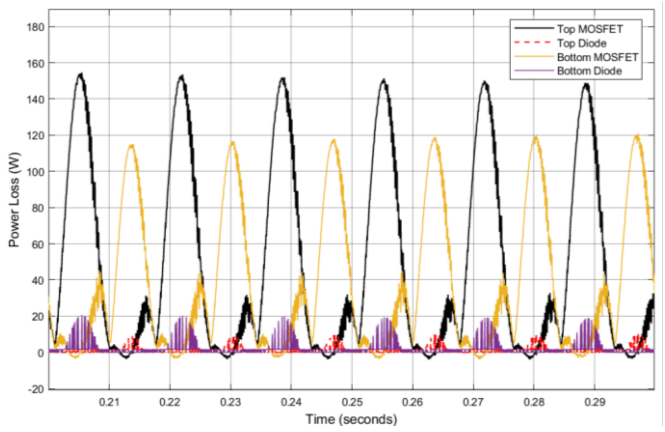

Fig. 7. Simulink heat generation inputs: Phase-A.

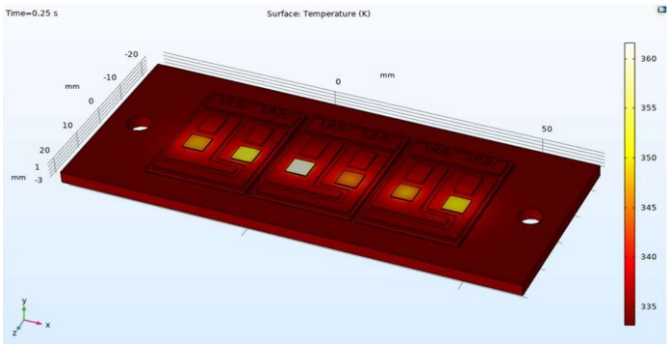

Fig. 8. COMSOL thermal simulation of a CREE CCS050M12CM2 SiC MOSFET power module.

seen in Fig. 6 has not decreased in thickness but has decreased 60% in conducting cross-sectional area to the point where the conducting region is further inward than the edge of the chip. The square chips at the top of the transistor stacks seen in Fig. 4 are the SiC MOSFETs used in the module while the rectangular chips above the MOSFETs are the SiC free-wheeling diodes used in conjunction with the MOSFETs. Each diode and MOSFET has a heat generation curve associated with a specific operating condition. The heat generation curves for each of the SiC MOSFETs and diodes were created in Matlab/Simulink with the add-on Simscape. This environment has a transistor MOSFET model that will output the power loss the transistor will experience depending on the simulated circuit. A sine-triangle pulse-width modulation switching scheme was used with the inverter to drive an induction motor load. The inverter used a 400 V DC-link voltage, 60 A peak sinusoidal output current, 5 kHz switching frequency, and 60 Hz line frequency. Shown in Fig. 7 is Phase-A of power loss or heat generation outputs from this simulation. Each phase consists of a top and bottom MOSFET and diode. The curves of each phase were used for the COMSOL thermal simulation shown in Fig. 8 with an ambient temperature of 60°C and a cooling convection coefficient with a value of 10,000 W/m^{2}K applied to the bottom of the baseplate.

The results in Fig. 9 demonstrate three RBFNs trained on the center, side, and middle points shown in Fig. 2 for the left MOSFET chip of the left material stack in Fig. 4. The results in column (a) of Fig. 9 correspond to the point on the baseplate underneath the center of the MOSFET chip. The results in column (b) of Fig. 9 correspond to the point on the baseplate to the side of the MOSFET chip underneath the outer perimeter of the solder layer. The results in column (c) of Fig. 9 correspond to the midpoint between the two points considered in column (a) and column (b). The first row of plots shows the comparison between the healthy baseplate temperature training data from COMSOL and the output of the trained RBFN. The second and third rows of plots show the comparison between the trained RBFN and the unhealthy temperature data for a whole second of data. The fourth row of plots shows the MSE between the trained RBFN and the unhealthy data at every point across the entire simulation range with the MSE plotted logarithmically. Comparisons between different error statistics

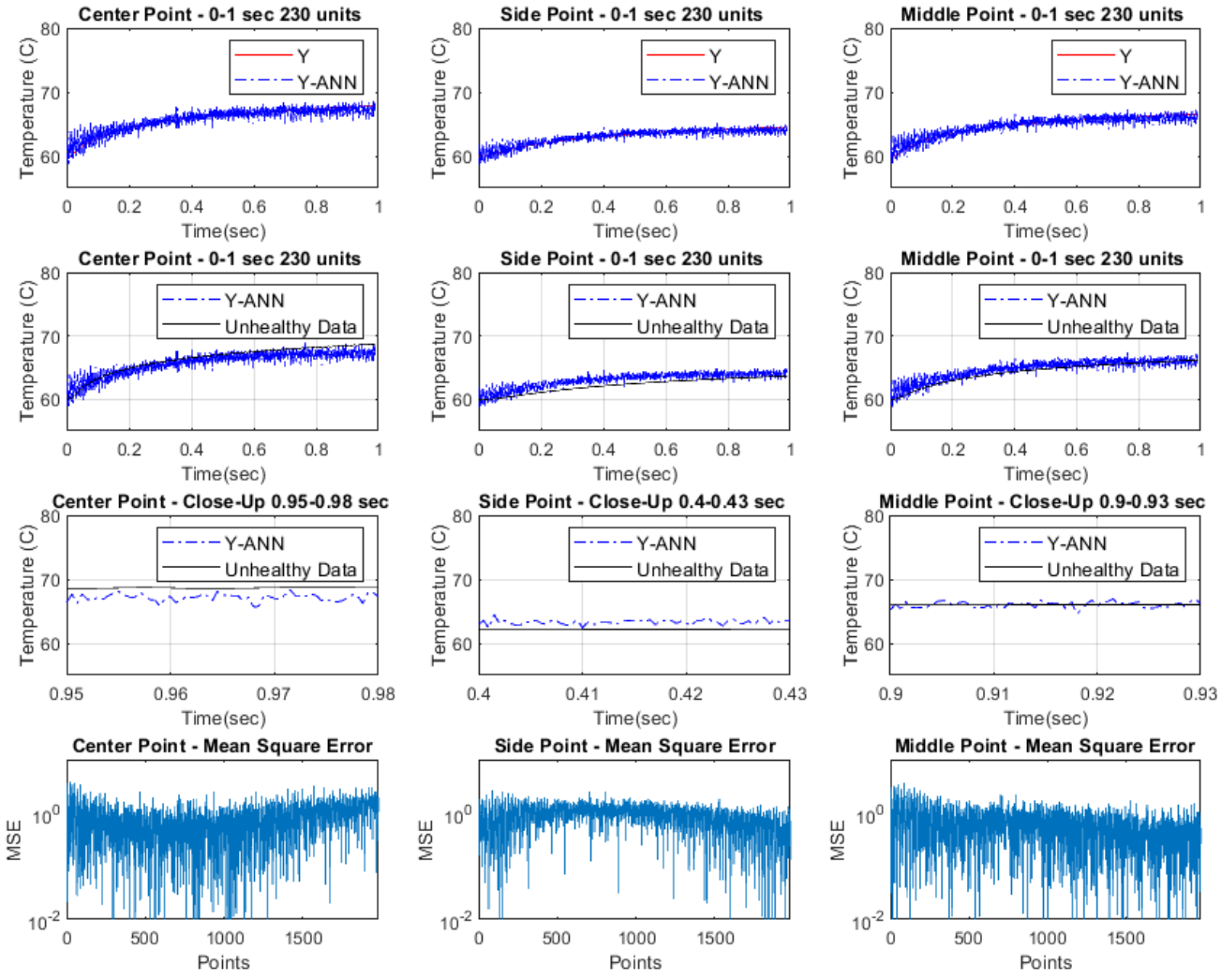

Fig. 9. Comparisons of trained RBFN and FEA temperature data at (a) center point, (b) side point, and (c) middle point.

Table. I: Error Comparisons between Center, Side, and Middle Points.

Point On Module	Y & Y-ANN MSE (°C)	Y & Unhealthy MSE (°C)	Y-ANN & Unhealthy MSE (°C)	Y-ANN & Unhealthy Max Temperature Difference (°C)	Y-ANN & Unhealthy Mean Error (°C)	Qualitative Description	Thresholds for Error	Y-ANN & Unhealthy Percentage Change
Center	0.5652	0.8104	1.2273	3.7831	1.2219	Increase	>1.75%	2.05%
Side	0.2831	0.9542	1.1103	2.5850	-1.1073	Decrease	>1.75%	1.85%
Middle	0.4884	0.4152	0.4045	3.4942	0.0535	Constant	<1%	0.6%

for the center, side, and middle points can be seen in Table I. The maximum averaged mean squared error (MSE) for a sequence of 200 points was found between the healthy output *Y*, the unhealthy output, and the trained RBFN output *Y-ANN*. The trained RBFN can be seen to follow the healthy data well in the first row of plots, with an MSE of 0.5652°C, 0.2831°C, and 0.4884°C for the center, side, and middle points, respectively. The MSE between *Y-ANN* and the unhealthy output for the three points indicates a substantial increase in temperature for the center point, a decrease in temperature for the side point, and a consistent temperature for the middle point. The temperature differences all indicate a solder crack fault has occurred when using the listed thresholds in Table I as markers for diagnosis. Diagnosis of the solder fault can be further strengthened by noting the time of maximum temperature difference at 1 second and 0.4 seconds for the center and side points, respectively.

IV. Conclusions and Future Work

This study explored the effectiveness of using an RBFN to monitor for changes in the thermal distribution across an SiC MOSFET power module to identify the existence of solder cracks in the module. The RBFN was trained using healthy FEA thermal simulation data. The output of the RBFN was then compared to the unhealthy FEA simulation data at three specific points on the baseplate of the power module. As solder cracks expand from the outer edges of the solder layer towards the center of the module, constricting the heat flow inwards, the temperature at different points on the baseplate changes as well. The comparison between the trained RBFN and the unhealthy FEA simulation data shows significant changes in temperature on the baseplate depending on the location. The future work for this study lies in incorporating more power module operational states to provide a more accurate heathy model as well as investigating a way to update the parameters of the healthy model once a fault is detected for continued monitoring.

References

[1] J. Millan, P. Godignon, X. Perpina, A. Perez-Tomas, and J. Rebollo, "A survey of wide bandgap power semiconductor devices," *IEEE Trans. Power Electronics*, vol. 29, no. 5, pp. 2155–2163, May 2014.

[2] M. Ciappa, "Selected failure mechanisms of modern power modules," *Microelectronics Reliability*, vol. 42, no. 4–5, pp. 653–667, 2002.

[3] B. Lu and S. K. Sharma, "A literature review of IGBT fault diagnostic and protection methods for power inverters," *IEEE Trans. Industry Applications*, vol. 45, no. 5, pp. 1770–1777, Sept.-Oct. 2009.

[4] Z. J. Shen and I. Omura, "Power semiconductor devices for hybrid, electric, and fuel cell vehicles," *Proc. IEEE*, vol. 95, no. 4, pp. 778–789, 2007.

[5] C. Van Godbold, V. A. Sankaran, J. L. Hudgins, and S. Member, "Thermal analysis of high-power modules," *IEEE Trans. Power Electronics*, vol. 12, no. 1, pp. 1–10, Jan. 1997.

[6] A. Morozumi, K. Yamada, T. Miyasaka, S. Sumi, and Y. Seki, "Reliability of power cycling for IGBT power semiconductor modules," *IEEE Trans. Industry Applications*, vol. 39, no. 3, pp. 665–671, May-Jun. 2003.

[7] Z. Wang, W. Qiao, B. Tian, and L. Qu, "An effective heat propagation path-based online adaptive thermal model for IGBT modules," in *Proc. IEEE Applied Power Electronics Conf. Expo.*, Mar. 2014, pp. 513–518.

[8] K. B. Pedersen and K. Pedersen, "Bond wire lift-off in IGBT modules due to thermomechanical induced stress," in *Proc. 3rd IEEE International Symposium on Power Electronics for Distributed Generation Systems*, Jun. 2012, pp. 519-526.

[9] N. Dornic et al., "Stress-Based Model for Lifetime Estimation of Bond Wire Contacts Using Power Cycling Tests and Finite-Element Modeling," in *IEEE Journal of Emerging and Selected Topics in Power Electronics*, vol. 7, no. 3, pp. 1659-1667, Sept. 2019.

[10] S. Yang, D. Xiang, A. Bryant, P. Mawby, L. Ran, and P. Tavner, "Condition monitoring for device reliability in power electronic converters: A review," *IEEE Trans. Power Electronics*, vol. 25, no. 11, pp. 2734-2752, Nov. 2010.

[11] P. Beckedahl, "Advanced power module packaging for increased operation temperature and power density," in *Proc. 15th International Power Electronics and Motion Control Conference*, Sept. 2012, pp. Session 4-1-Session 4-5.

[12] K. Wei, W. Wang, Z. Hu, and M. Du, "Condition monitoring of IGBT modules based on changes of thermal characteristics," *IEEE Access*, vol. 7, pp. 47525-47534, 2019.

[13] Z. Wang, B. Tian, W. Qiao, and L. Qu, "Real-time aging monitoring for IGBT modules using case temperature," *IEEE Trans. Industrial Electronics*, vol. 63, no. 2, pp. 1168-1178, Feb. 2016.

[14] C. Sbarufatti, M. Corbetta, M. Giglio, and F. Cadini, "Adaptive prognosis of lithium-ion batteries based on the combination of particle filters and radial basis function neural networks," *J. Power Sources*, vol. 344, pp. 128–140, Jan. 2017.

[15] G. Sideratos and N. D. Hatziargyriou, "Probabilistic wind power forecasting using radial basis function neural networks," *IEEE Trans. Power Systems*, vol. 27, no. 4, pp. 1788-1796, Nov. 2012

[16] Y. Wu, H. Wang, B. Zhang, and K.-L. Du, "Using radial basis function networks for function approximation and classification," *ISRN Applied Mathematics*, vol. 2012, no. 324194, Mar. 2012.

[17] X.-F. Li, J.-H. Dong, and Y.-Z. Zhang, "Modeling and applying of RBF neural network based on fuzzy clustering and pseudo-inverse method," in *Proc. International Conference on Information Engineering and Computer Science*, Dec. 2009, pp. 1-4.

[18] M. Mohammadi, N. S. A. Krishna, and S. K. Nandy, "A hardware architecture for radial basis function neural network classifier," *IEEE Trans. Parallel and Distributed Systems*, vol. 29, no. 3, pp. 481-495, Mar. 2018.

[19] CREE, "CCS050M12CM2 1.2kV, 25mΩ All-Silicon Carbide Six-Pack (Three Phase) Module," CCS050M12CM2 datasheet, Jan. 2018.

[20] C. Entzminger, W. Qiao, L. Qu, and J. Hudgins, "A high-accuracy, low-order thermal model of SiC MOSFET power modules extracted from finite element analysis via model order reduction," in *Proc. IEEE Energy Conversion Congress & Expo.*, Sept.-Oct. 2019, pp. 4950-4954.